Matrix Product States with Large Sites

Henrik R. Larsson,* Huanchen Zhai, Klaas Gunst, and Garnet Kin-Lic Chan*

Read Online

ACCESS | Metrics & More | Article Recommendations | Supporting Information

ABSTRACT: We explore various ways to group orbitals into clusters in a matrix product state (MPS). We explain how a generic cluster MPS can often lead to an increase in computational cost and instead propose a special cluster structure, involving only the first and last orbitals/sites, with a wider scope for computational advantage. This structure is a natural formalism to describe correlated multireference (MR) theories. We demonstrate the flexibility and usefulness of this approach by implementing various uncontracted MR configuration interaction, perturbation, and linearized coupled cluster theories using an MPS with large cluster sites. Applications to the nitrogen dimer, the chromium dimer, and benzene, including up to triple excitations in the external space, demonstrate the utility of an MPS with up to two large sites. We use our results to analyze the quality of different multireference approximations.
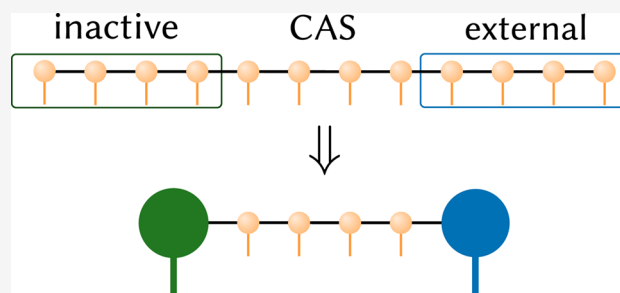
1. INTRODUCTION

The density matrix renormalization group (DMRG) and its associated ansatz of matrix product states (MPSs)[1−6] are established as useful electronic structure approximations in problems where there are a large number of correlated open shells.[7−13] The formalism requires first mapping the orbitals to a one-dimensional lattice of sites. One direction discussed already in the first quantum chemistry DMRG paper[14] is the possibility of grouping clusters of related orbitals into large "sites" (Figure 1), whose Hilbert space is then approximated outside of the truncation procedure of DMRG. Such a cluster MPS seems attractive for interpretation, as one can group orbitals corresponding to chemical identity, and it has been efficiently implemented in a number of works.[15−20] However, because the Hilbert space of the cluster site grows exponentially quickly with the number of cluster orbitals, the computational advantage is less clear. In addition, the drawbacks of clustering, which gives rise to more complicated interactions and entanglement between clusters, has been understood since the earliest formulations of the quantum renormalization group.[21,22] In the first part of this work, we analyze whether clustering orbitals is a good idea in chemical problems from the view of computational cost and accuracy.

In the second part, we discuss a specific setting where grouping sites into large clusters has a clear theoretical computational advantage. This occurs when the clusters are at either end of the DMRG lattice (Figure 2). Because the clusters do not share a common boundary, the cluster Hilbert space dimension appears together with the MPS bond dimension in a computationally more favorable way than in a general cluster MPS. A natural application for this type of MPS is to represent dynamical correlations by clustering inactive and external orbitals. As we demonstrate, this leads to a substantial cost reduction in MPS treatments of dynamic correlation.
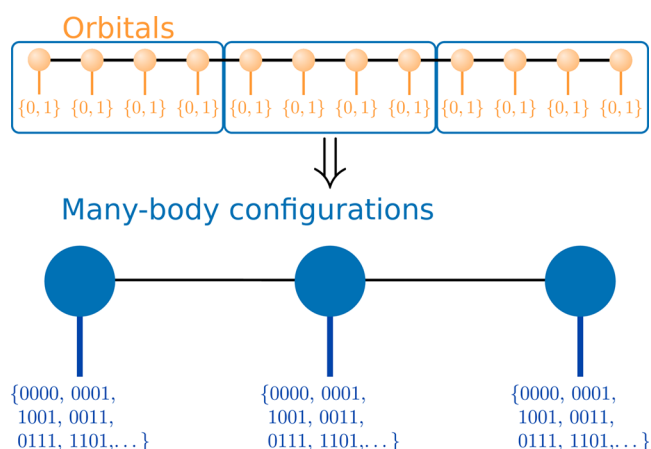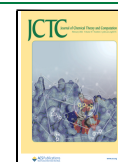

Figure 1. A cluster matrix product state obtained by combining multiple orbitals into large sites. The Hilbert space of each of the large sites consists of P many-body configurations that may be further approximated.[15]
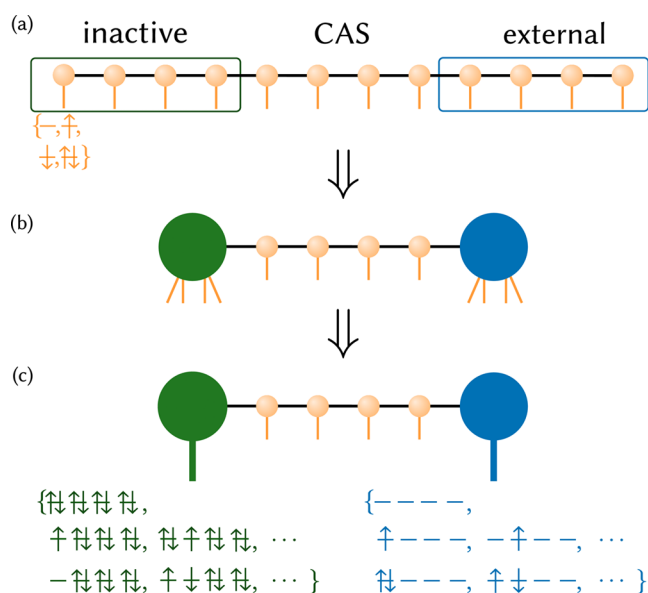
Figure 2. (a, b) Diagrammatic representation of a cluster MPS with two large sites at either end of the lattice. This ansatz demonstrates favorable scaling with respect to the large site Hilbert space dimension because there is no shared boundary between the large sites. (c) Application to an uncontracted multireference dynamic correlation wave function in the singles and doubles space, where the Hilbert space of the green site covers the inactive orbitals and the Hilbert space of the blue site covers the external orbitals.

The paper proceeds as follows. We start by analyzing the cost of cluster MPS (Section 2.1) and explain why computational gains are not expected in general settings. We then analyze the conditions leading to the favorable cost of the single and double cluster-site model (Section 2.2) and discuss its application to uncontracted multireference dynamic correlation theories (Section 2.3). We next discuss the detailed implementation of DMRG with large cluster sites in Section 3, taking advantage of the large-scale parallel DMRG implementation in ref 23. Finally in Section 4, we demonstrate the cluster MPS implementation of uncontracted multireference configuration interaction (MRCI), multireference perturbation theory (MRPT), and multireference linearized coupled cluster theories (MRLCC) in applications to the nitrogen dimer, chromium dimer, and the benzene molecule, using complete active spaces (CASs) with up to 30 electrons and 30 orbitals, with up to triples in the external space, and with up to 280 external orbitals. We conclude in Section 5.

Note: while this manuscript was under review, a related preprint appeared that implements uncontracted MRCI by using an MPS with a single cluster site.[24]

2. THEORY

2.1. Analysis of Clustering Sites in Matrix Product States. The benefit of clustering orbitals depends on the entanglement structure of the problem. If the entanglement is such that groups of sites are strongly entangled internally, but only weakly entangled between the groups, then it may make sense computationally to cluster into large sites. The critical question is how large this difference in intra- versus intercluster entanglement needs to be for a computational benefit.

To start, we recall the computational cost of the standard DMRG algorithm and then examine the cost for multiple clusters of sites and, then finally, for large sites at the ends of the DMRG lattice, the latter being the main focus in this work.

2.1.1. Standard Matrix Product States. In the standard MPS/DMRG formulation, the wave function for K orbitals is mapped to a lattice of K sites and written as a matrix product state (MPS) of bond dimension D,[1]

$$|\Psi\rangle = \sum_{\{n_i\}} \mathbf{A}^{n_1}\mathbf{A}^{n_2}\ldots\mathbf{A}^{n_K}|n_1 n_2 \ldots n_K\rangle \tag{1}$$

where the matrices $\mathbf{A}^{n_i}$ at "site" i are of dimensions $D_i \times D_{i+1}$, except those associated with the first and last sites, which are vectors of size D_i. The bond dimension of the MPS is then defined as $D = \max_i D_i$. The local Hilbert space $\{|n\rangle\}$ is that of a spatial orbital ϕ and the dimension is $P = 4$ ($\{|n_i\rangle\} = \{|\text{vac}\rangle, |\phi_i^\alpha\rangle, |\phi_i^\beta\rangle, |\phi_i^\alpha \phi_i^\beta\rangle\}$).

The main cost of the DMRG algorithm when using electronic structure Hamiltonians stems from two steps, performed at each site: (1) the construction and diagonalization of an effective Hamiltonian in the product space of one or more sites and the renormalized Hilbert space of their environment and (2) the transformation of operators into the new renormalized space.[14,25] Both steps contribute to the leading computational scaling, which is usually given (per site) as $O[(K_<^2 + K)D^3P^2 + K_<^2 K_> D^2]$, assuming $D_i \sim D$. $K_< (K_>)$ is the smaller (larger) of the numbers of orbitals to the left and right of the bipartition at site i. In the following, we assume that $D \gg K$ in order to drop the second term, which stems from the transformation of operators. In addition, as $P = 4$ is a small constant, we drop the P dependence for a standard MPS. For the total cost, $K_{</>} \sim K$, and the cost per site is then multiplied by K to obtain the leading cost for the DMRG algorithm of $O[K^3D^3]$. For reference, the precise scalings for a

Table 1. Comparison of the Scaling for the Computational Cost of the Various MPS-Based DMRG Formulations[a]

method	diagonalization and renorm. operators	compl. renorm. op.
normal MPS	K^3D^3	K^4D^2
cluster MPS	$CK^2[D^3P + D^2\text{poly}(P)]$	CK^3D^2
single large site MPS	$K_{\text{act}}(K_{\text{act}}^2 + K)D_{\text{act}}^3 + (K_{\text{act}}^2 + K)[D_{\text{ext}}^2 P + D_{\text{ext}}\text{poly}(P)]$	$K_{\text{act}}^2 K D^2$
MPS-MRCISD (large site MPS)	as single large site MPS with $P = K_{\text{ext}}^2$	
MPS-MRCISD (conventional MPS)	$K_{\text{act}}(K_{\text{act}}^2 + K)D_{\text{act}}^3 + \sum_{i=K_{\text{act}}}^{K}(K_{<,i}^2 + K)D_i^3$	$K_{\text{act}}^2 K D^2 + \sum_{i=K_{\text{act}}}^{K} K_{<,i}^2 K_{>,i} D_i^2$

[a]D defines the bond dimension, K the number of orbitals, P the number of configurations on the large site, and C the number of clusters (large sites) in a cluster MPS. For the MPS with large sites at either ends, we here assume only one large site with K_{ext} orbitals, for simplicity. The number of standard (orbital-based) sites is then K_{act} and $K_{\text{ext}} + K_{\text{act}} = K$. The first column shows the costs for carrying out the Davidson diagonalization and operator renormalization steps, while the second column is an additional cost for the complementary operator renormalization step.

normal MPS and different variations of MPSs discussed below are gathered in Table 1.

2.1.2. Cluster Matrix Product States. The above analysis can be repeated for a cluster MPS with clusters of orbitals as sites. We assume that each cluster has K_c orbitals, with a cluster Hilbert space of P configurations. Then the number of sites in the cluster MPS is reduced to $K/K_c = C$. To simplify the analysis, we assume that K_c is similar for all clusters. Note that to obtain the same accuracy as the standard MPS, the bond dimension used between two clusters must be the same as the bond dimension in the standard MPS between the sites at the boundary of the two clusters. Now consider increasing the number of orbitals in each cluster K_c. Assuming the full Hilbert space of each cluster is used, then $P \sim 4^{K_c}$. Because P is now potentially large, we consider it as important as D and K in the analysis of the leading scaling.

The cost of the cluster MPS is then given by $O\{CK^2[D^3P + D^2\text{poly}(P)] + CK^3D^2\}$, analogous to the standard MPS cost. We again assume that $D \gg K$ and drop the last term. In contrast to the cost given above for the standard MPS, here we have written the first term without a P^2 dependence because we assume the use of a tripartition to perform the diagonalization and renormalization. As explained below in Section 3.3, this changes the cost of the first term per site from $O(K_<^2 D^3 P^2)$ to $O(K_< K_> D^3 P)$. The term containing poly(P) stems from applying operators in the cluster space onto the site and is at most P^2. However, in many common situations we can use a local basis (such as a determinantal basis) in which the Hamiltonian is sparse. Then poly(P) $\sim P$. Hence, the leading cost of the cluster MPS simplifies to $O(CK^2D^3P)$.

While P only appears linearly in the scaling, it grows much faster than the $1/K_c$ reduction in the number of sites in the cluster MPS. Although there are ways to truncate the cluster Hilbert space, e.g., via filtering determinants ("selected configuration interaction"),[15] general linear subspace projection ("Tucker decomposition"),[26] or using an additional factorized ansatz for the MPS cluster matrix ("comb tensor networks"),[16,27] any choice must achieve an effective exponential reduction in P complexity, to compete with the standard MPS cost. This means that in systems whose entanglement is well described by a standard MPS with constant bond dimension across the lattice, a cluster MPS is unlikely to reduce computational cost for the same accuracy.

A different limiting case is in problems described by an MPS with highly nonuniform bond dimensions, large within a cluster of sites and very small between clusters. The extreme case is no entanglement ($D = 1$) between clusters, i.e., the state is a product state of cluster wave functions (such as a generalized valence bond wave function, or for infinitely separated or noninteracting systems).[18,20,28,29] Since $D = 1$, it does not appear in the scaling and we need to consider terms nonleading in D in the analysis. Assuming determinant-like sparsity in the local basis, the DMRG cost is then $O[C(K^2P + K^3)]$. Conversely, when treating the problem using a standard MPS, $D > 1$ when cutting across a cluster. In the worst case, $D \sim O(P^{1/2})$, yielding $O(CK^2P^{3/2})$ cost (the leading D term). This is larger than the cluster MPS result because we assumed no compressibility within the cluster, and the renormalized MPS basis cannot use sparsity. Thus, the cluster MPS is advantageous in this limit.

In general, chemical problems fall between these two limiting cases. Sufficiently weakly interacting units are close to the second limiting case, and thus there are computational benefits to using the cluster MPS there. But the exponential overhead of clustering, together with the presence of long-range interactions (which introduce long-range entanglement) means that many problems are in fact close to the first scenario. To illustrate this, in the Appendix we carry out numerical simulations using both cluster MPS as well as the ordinary MPS for hydrogen chains at several geometries. The results show that there can be little gain from clustering even in a regime where the chemical identity of individual atoms or molecular units is evident.

2.2. Matrix Product States with Large Sites at the Ends. We now turn to the case of main interest in this work, when there are large sites at one or both ends of the MPS lattice. In anticipation of the multireference use-cases discussed later, the orbitals treated in the usual MPS fashion will be denoted active orbitals, orbitals in the left cluster will be denoted inactive, and orbitals in the right cluster will be denoted external. The number of orbitals in each class is then K_{act}, K_{inact}, and K_{ext}, respectively. The ansatz thus takes the form (see also Figure 2).

$$|\Psi\rangle = \sum_{\{n\}} \mathbf{A}^{\mathbf{n}_{\text{inact}}} \mathbf{A}^{n_{K_{\text{inact}}+1}} \mathbf{A}^{n_{K_{\text{inact}}+2}} \dots \mathbf{A}^{\mathbf{n}_{\text{ext}}}$$
$$|\mathbf{n}_{\text{inact}} n_{K_{\text{inact}}+1} n_{K_{\text{inact}}+2} \dots \mathbf{n}_{\text{ext}}\rangle \tag{2}$$

where $\mathbf{n}_{\text{inact}}$ and $\mathbf{n}_{\text{ext}}$ label the Hilbert space of the inactive and external sites of dimension P_{inact}, P_{ext}, respectively.

To simplify the scaling discussion, we will ignore the left large site, i.e., $K_{\text{inact}} = 0$. The main finding is easily generalized to the case of $K_{\text{inact}} \neq 0$. Following the discussion above, the DMRG cost at sites within the active space is the same as in standard DMRG, i.e., $O[(K_{\text{act}}^2 + K)D^3P^2]$ ($P = 4$), where the only difference is that $K_{\text{act}} \neq K$. The new consideration is for the site at the boundary between the active sites and the large external site. The contraction at the boundary has cost $O[(K_{\text{act}}^2 + K)[D_{\text{ext}}^2 P_{\text{ext}} + D_{\text{ext}}\text{poly}(P_{\text{ext}})]]$ where D_{ext} is the bond dimension at the boundary. As for the cluster MPS, we assume poly(P_{ext}) $\sim P_{\text{ext}}$ and drop the last term. Unlike in the general cluster MPS, however, the cluster Hilbert space dimension appears with D_{ext}^2, not D_{ext}^3. Thus, for P_{ext} not too large (see below) it is possible to obtain a speedup. For the case of two large sites we must also consider the boundary between the inactive large site and the active space, but this takes the same form where the inactive cluster Hilbert space dimension is multiplied by D_{inact}^2. In the limiting case of $K_{\text{act}} = 0$, i.e., the MPS consists of only two large sites, the cost scales as $O[(K_{\text{Int}}^2 + K_{\text{ext}})D_{\text{ext}}^2 P_{\text{ext}}]$. This corner case may be advantageous when P_{ext} is small enough, but will not be considered further here.

One concrete application is to use the ansatz eq 2 to represent orbital partitioned quantum chemistry models, such as the restricted active space (RAS) model and other uncontracted multireference dynamic correlation models. For example, if we assume a singles and doubles theory where the external space contains at most two electrons, then $P_{\text{ext}} \sim K_{\text{ext}}^2$. With the use of a standard MPS to represent such a state, the external space restriction limits the bond-dimension of the MPS to D_{ext} at the boundary. The cost of the standard DMRG contraction at the boundary site is $O(K_{\text{ext}}^2 D_{\text{ext}}^3 P^2)$ (with $P = 4$),

and assuming D_{ext} decreases linearly across the external orbitals, the leading cost becomes $O(K_{ext}^3 D_{ext}^3)$ (the precise scaling is detailed in Table 1). However, using a large external site, and the expression for the single boundary contraction, then for $K_{ext} \sim K > K_{act}^2$ we obtain a speedup of D_{ext} relative to the standard DMRG implementation. If $K_{ext} < K_{act}^2$, the speedup will be larger than $\sim D_{ext}/K_{ext}$. For an external space with only single excitations out of the active space, the speedup is even greater, namely up to KD_{ext}. For a more general external space, e.g., constructed by selected configuration interaction,[30−33] a similar analysis can be applied.

2.3. Matrix Product State Formulation of Uncontracted Dynamical Correlation Methods. We next describe how to approximate various uncontracted multireference dynamical correlation methods using MPS. In all these cases, the large site MPS ansatz (2) can be used, and when the excitation degree is small (e.g., up to singles and doubles, in some cases up to triples), we can expect speedup relative to the standard MPS formulation. This will be assessed in the benchmark in Section 4.

2.3.1. Multireference Configuration Interaction Theory. The uncontracted multireference CI (uc-MRCI) ansatz takes the form

$$|\Psi_{uc-MRCI}\rangle = \sum_{C}^{n_{ref}} c_C|C\rangle + \sum_{E} c_E|E\rangle \tag{3}$$

where $|C\rangle$ denotes a configuration from the reference space (no particles in the external space, no holes in the inactive space) and $|E\rangle$ are configurations outside of the reference space, classified as singles (one particle in the external space), doubles (two particles in the external space), and so on. The uc-MRCI coefficients c_C and c_E are determined by minimizing the variational energy.

MRCI does not give an extensive energy, e.g., the energy of independent subsystems is not the sum of the energy of the systems. Defining the correlation energy as $\Delta E = E_{MRCI} - E_0$ (E_0 being the energy of the reference wave function $|\Psi_0\rangle = \sum_C c_C^0|C\rangle$, with c_C^0 determined variationally), the following approximate size-extensivity corrections have been defined (among others[34]):

$$E_D = (1 - c_0^2)\Delta E \tag{4}$$

$$E_{RD} = (1 - c_0^2)/c_0^2 \Delta E \tag{5}$$

$$E_P = \frac{\sqrt{N_{el}^2 + 2N_{el}\tan(2\theta)} - N_{el}}{2[\sec(2\theta) - 1]}\Delta E$$

$$\approx (1 - 2/N_{el})E_{RD}, \quad \theta = \arccos(c_0) \tag{6}$$

$$E_M = g_M E_{RD}, \quad g_M = \frac{(N_{el} - 2)(N_{el} - 3)}{N_{el}(N_{el} - 1)} \tag{7}$$

where E_D (E_{RD}) is the (renormalized) Davidson correction,[34,35] E_P is the Pople correction,[36] and E_M is the Meissner correction.[37] N_{el} is the number of correlated electrons, and c_0^2 is either defined as[38]

$$c_0^2 = \sum_C^{n_{ref}} c_C^2 \tag{8}$$

or as[39]

$$c_0^2 = \langle\Psi_0|\Psi_{MRCISD}\rangle^2 \tag{9}$$

Here, we use eq 8, which has been found to be slightly more accurate in many situations.[34,40] The size-consistency-corrected MRCI methods will be referred to as MRCI+Q$_X$, where X stands for the particular correction used.

One can also define an energy functional to variationally minimize that includes the size-extensivity correction in its definition. This permits a simple implementation of the gradients and properties. Many such functionals can be obtained by shifting the diagonal of the MRCI Hamiltonian according to

$$\hat{H} \rightarrow \hat{H} + \Delta\hat{P}, \quad \Delta = (1 - g)\Delta E \tag{10}$$

where

$$\hat{P} = \sum_E |E\rangle\langle E| \tag{11}$$

and the parameter g defines the type of correction.[34] Here, we will use only two variants $g = 1 - g_M$ (MR-averaged quadratic coupled-cluster, MR-AQCC, method[41]) and $g = 2/N_{el}$ (MR averaged coupled pair functional, MR-ACPF).[42] MR-AQCC is related to E_M and MR-ACPF is related to E_P, and MR-ACPF is extensive for identical subsystems.

The MPS versions of the above theories are easily defined, by constraining MPS to preserve constraints in the inactive and external Hilbert spaces. We will refer to the MPS versions of the above theories by prepending MPS to the name of the method, e.g., MPS-MRCI, MPS-ACPF, MPS-AQCC, etc. For brevity, we avoid the additional "uc" prefix and assume that "MPS-MRX" implies an uncontracted multireference formulation of method X.

2.3.2. Multireference Perturbation Theory and Multireference Coupled Cluster theory. It is straightforward to formulate uncontracted multireference perturbation theory in terms of MPS. This was discussed in ref 43 with subsequent extensions in refs 44−47. Given a zeroth-order Hamiltonian, $\hat{H}_0$, the first-order perturbed wave function, $|\Psi_1\rangle$, can be obtained by minimizing the Hylleraas functional[48]

$$H[|\Psi_1\rangle] = \langle\Psi_1|\hat{H}_0 - E_0|\Psi_1\rangle + 2\langle\Psi_1|\hat{Q}(\hat{H} - \hat{H}_0)|\Psi_0\rangle \tag{12}$$

where $\hat{Q} = 1 - |\Psi_0\rangle\langle\Psi_0|$. The MPS formulation corresponds to representing both $|\Psi_0\rangle$ and $|\Psi_1\rangle$ as MPS, approximating the uncontracted perturbation solution. The energy for third-order MRPT can be obtained from

$$E_{PT3} = E_{PT2} + \langle\Psi_1|\hat{H} - \hat{H}_0|\Psi_1\rangle \tag{13}$$

In ref 43, the above theory was implemented for the Dyall Hamiltonian[49] to approximate the uncontracted n-electron valence-state perturbation theory (NEVPT2),[50−52] and the resulting formulation was termed MPS-PT2. The Dyall Hamiltonian $\hat{H}_{0,D}$ is defined as[49,52]

$$\hat{H}_{0,D} = \sum_{ij\in inactive} F_{ij}\hat{a}_i^\dagger\hat{a}_j + \sum_{rs\in ext} F_{rs}\hat{a}_r^\dagger\hat{a}_s + \sum_{ab\in act} h_{ab}^{eff}\hat{a}_a^\dagger\hat{a}_b$$

$$+ \frac{1}{2}\sum_{abcd\in act} \langle ab|cd\rangle\hat{a}_a^\dagger\hat{a}_b^\dagger\hat{a}_d\hat{a}_c + E_D \tag{14}$$

$$h_{ab}^{eff} = h_{ab} + \sum_{i\in inactive} [2\langle ai|bi\rangle - \langle ai|ib\rangle] \tag{15}$$

$$E_D = 2 \sum_{i \in \text{inactive}} (h_{ii} - F_{ii}) + \sum_{ij \in \text{inactive}} [2\langle ij|ij\rangle - \langle ij|ji\rangle]$$

(16)

where $\mathbf{F}$ is the generalized Fock matrix. $h_{ij} = \langle i|h|j\rangle$ are the one-particle Hamiltonian matrix elements and $\langle ab|cd\rangle$ the electron repulsion matrix elements.

In ref 44, Fink's restraining the excitation degree (RE) Hamiltonian,[53,54]

$$\hat{H}_{0,F} = E_0 + \sum_{pq;\Delta n_{\text{ex}}=0} h_{pq}\hat{a}_p^\dagger \hat{a}_q + \frac{1}{2} \sum_{pqrs;\Delta n_{\text{ex}}=0} \langle pq|rs\rangle \hat{a}_p^\dagger \hat{a}_q^\dagger \hat{a}_s \hat{a}_r$$

(17)

was used, leading to an MPS-based version of RE perturbation theory (REPT). $\Delta n_{\text{ex}} = 0$ indicates that excitations between the inactive, active, and external spaces are omitted, compared to the full Hilbert space. If there is no active space, then $|\Psi_0\rangle$ is a single Slater determinant, and the result from REPT2 is identical to the linearized-coupled cluster (LCC) approximation, thus this approximation was termed MPS-LCC in ref 44. However, given a multireference $|\Psi_0\rangle$, this equivalence no longer holds. We will consider another linearized multireference coupled cluster approximation below, thus we will refer to this choice of $\hat{H}_{0,F}$ as MPS-MRREPT2.

Refs 55 and 56 defined the first linearized multireference coupled cluster approximation (MR-LCCM). This corresponds to the choice

$$H_{0,\text{LCCM}} = \hat{P}\hat{H}\hat{P} + |\Psi_0\rangle\langle\Psi_0|E_0|\Psi_0\rangle\langle\Psi_0|$$

(18)

where $\hat{P}$ is defined in eq 11 and $|\Psi_1\rangle$ is solved for only in the excited space, i.e., $|\Psi_1\rangle = \hat{P}|\Psi_1\rangle$. It differs from REPT2 in that (a) $|\Psi_1\rangle$ has no contributions in the reference space and (b) the excitation spaces of degree $n_{\text{ex}} > 0$ are coupled in $\hat{H}_0$. We refer to the MPS implementation of this theory as MPS-MRLCCM.

3. IMPLEMENTATION

We have implemented the modified MPS algorithms described above in several ways. We have implemented uncontracted dynamical correlation methods within a standard MPS formulation by restricting the occupancy of different spaces, as described in Section 3.1 within BLOCK2.[23] The large site implementation of the dynamical correlation methods is implemented in BLOCK2 as well, as described in Section 3.2. Finally, the general cluster MPS (used in the computations in the Appendix) is implemented within the DMRG program SCHWARZBROT[18] as described in Section 3.3. For general references on DMRG implementation, we refer to the literature.[4,23,25,57−60] The above MPS algorithms are interfaced with the PySCF program.[61,62]

3.1. Restricting Configurations in Matrix Product States. To implement the unrestricted multireference dynamical correlation theories in Section 2.3 in a standard MPS, we enforce constraints on the MPS matrices. Elementary symmetries such as particle number or spin symmetry are usually taken into account by introducing irreducible blocks in the MPS site matrices $\mathbf{A}^{n_i}$,[1,6,25,63] where each block corresponds to a different symmetry (e.g., number of particles) to the left and right of the given site. If the MPS sites are ordered according to the orbital spaces, inactive (K_{inact}), active (K_{act}), and external (K_{ext}), the same technique can be used to constrain the MPS ansatz to a wave function of the form (3) with a given excitation level. For example, restricting the

particle numbers on site $i \leq K_{\text{inact}}$ to be $\{i, i-1, i-2\}$ and the particle numbers on site $i > K_{\text{Int}}$ to be $\{N_{\text{el}}, N_{\text{el}} - 1, N_{\text{el}} - 2\}$, we approximate the ansatz (3) with singles and doubles excitations. We assume here that the inactive orbitals are placed on the left of the MPS and that the external orbitals are placed on the right of the MPS. The particle number then increases from site to site up to the total electron number, N_{el}, at the end of the last site. Corner cases are neglected. Particle number restriction is sufficient to implement the uncontracted multireference dynamical correlation approaches in this work, but extensions to other symmetry sectors (e.g., S_z and S^2 symmetry) is possible, and can, for example be used to describe wave functions restricted by the seniority quantum number.[63] In passing, we note that this approach is very different from the "multilevel" DMRG,[64] where different maximal bond dimensions are used in the three subspaces, without any restrictions on the particle number blocks.

3.2. Matrix Product States with Large Sites in the Ends. Introducing large sites in an MPS requires significant changes in the implementation of a DMRG code. Since for conventional MPSs in electronic structure theory, the physical dimension of a site is $P = 4$, or, with spin−orbital sites, even 2, one typically does not optimize the DMRG implementation around the size of the physical dimension. However, for large sites, P can become arbitrarily large. Hence care must to be taken to avoid unfavorable costs and scaling with respect to P.

In standard CI methods, the matrix representation of operators is seldom explicitly constructed, and instead, matrix vector products, such as $\hat{H}|\Psi\rangle$, are evaluated on the fly. Here, however, we store all required operators that act in the large site Hilbert space and represent them as sparse matrices (in the determinantal basis of the large site) of size $P \times P$. This is because (a) operators in DMRG need to be accessed more often than in standard CI methods and (b) the size of the large site basis is small ($\sim10^6$), compared to standard CI methods. Note that the determinantal configurations range over different numbers of electrons (e.g., between 0 and 2 for the external site in an implementation of the multireference singles and doubles theories), and this yields extremely sparse operator matrices depending on the operator, e.g., with $O(P)$ or even $O(1)$ nonzeros. In our implementation, for up to two electrons in the external space, most of the memory and runtime (including the initialization) is spent on optimizing the regular sites in the active space and not the large inactive or external sites.

A standard DMRG implementation uses a decomposed form of the Hamiltonian $\hat{H} = \sum_\alpha \hat{O}_L^\alpha \hat{O}_R^\alpha$ to carry out the optimization of the MPS matrix at a given site, where $\hat{O}_L^\alpha$, $\hat{O}_R^\alpha$ define operators that act to the left/right (inclusive) of the given site. There are multiple such decompositions,[23] e.g., we can group the Hamiltonian integrals with either the left or right operator, resulting in a normal (no integrals) or complementary (with integrals) operator. When approaching the site in the middle of an MPS during a sweep, it is advantageous in the standard algorithm to swap the assignment of normal and complementary between the left and right operators in order to reduce the number of terms in the α sum.[23,65,66] In the large site implementation of multireference dynamic correlation, this is not required, because we can usually assume that $K_{\text{ext}} \gg K_{\text{inact}} + K_{\text{act}}$, and thus the sweep is always over the first "half" of the sites. In practice, this means that only the normal operators are constructed for the inactive and active sites, and only the

753

complementary operators are constructed for the last external site.

The standard DMRG algorithm extracts a renormalized basis at each site by constructing and diagonalizing a density matrix.[2,25] Small perturbations are also added to this density matrix to improve convergence during the optimization.[67] For the large site, however, the density matrix would have size $O(P^2)$. To avoid constructing this large object, we use the singular value decomposition (SVD) of the large site, $\mathbf{A}^{\mathbf{n}_{ext/inact}}$, which reduces the scaling of the memory to $O(DP)$.[68,69] Finally, standard DMRG simulations often use a two-site algorithm where two adjacent sites are optimized simultaneously, in order to improve convergence and to optimize the distribution of symmetry blocks in each MPS matrix. We use a two-site algorithm on all sites except the large sites, which are treated using the one-site algorithm. To ensure that symmetry sectors in each matrix are not lost during the DMRG sweep, we always retain at least one state in each symmetry sector (particle number, point group, and S_z) in the SVD. Our large site implementation does not currently use S^2 symmetry.

To evaluate the scalar size-extensivity energy corrections, the weight of the reference space, c_0^2, is required. An evaluation as eq 9 via $|\langle \Psi_0 | \Psi_{MRCISD} \rangle|^2$ is done by straightforward contraction of two MPSs.[1] An evaluation as eq 8 via $\sum_C c_C^2$ requires first setting the inactive and external configurations in the MPS ansatz (2), $\mathbf{n}_{inact} = \{2_1 \dots 2_{K_{inact}}\}$, $\mathbf{n}_{ext} = \{0_1 \dots 0_{K_{ext}}\}$, and then computing the norm by contracting the resulting MPS with itself. The energy functionals associated with the AQCC and ACPF methods are implemented by modifying the diagonal of the Hamiltonian during the optimization, as shown in eq 10. We shift the diagonal of $\hat{H}$, excluding the reference space, by constructing a matrix product operator (MPO)[1,65] representation of $\hat{P}$ defined in eq 11, giving $\hat{H} \rightarrow \hat{H} + \Delta \hat{P}$. For ΔE, we evaluate the correlation energy using the lowest energy so far observed during the DMRG sweep.

The perturbation-based methods MPS-MRLCCM and MPS-MRREPT2 are implemented in the DMRG sweep algorithm by solving linear equations at each site instead of eigenvalue problems.[43] For MPS-MRLCCM, eq 18 can be constructed by removing the reference space in $|\Psi_1\rangle$. The zeroth-order Hamiltonian in MPS-MRREPT can be constructed by including only particle-number-conserving operators on the large sites.

3.3. Cluster Matrix Product States.
While the implementation of the cluster MPS follows that of an MPS with many large sites, more care has to be taken to avoid a P^2-type of computational cost. In addition to the modifications described in Section 3.2, all DMRG optimization sweeps are performed in the one-site mode and explicitly blocked operators (which act on the Hilbert space of a block enlarged by a site) are not explicitly constructed. (For example, this means that we always use a tripartition of the Hamiltonian $\hat{H} = \sum_\alpha \hat{O}_L^\alpha \, \hat{O}_S^\alpha \, \hat{O}_R^\alpha$ where the S index denotes the site being optimized in the sweep). This changes the $O(K_<^2 D^3 P^2)$ term in the scaling of operator multiplication at a site in the DMRG sweep to $O(K_< K_> D^3 P)$, c.f. Section 2.1.2.

4. APPLICATIONS

4.1. Nitrogen Dimer.
Here, we compare relative timings of (a) a standard DMRG computation (approximating full configuration interaction, FCI), (b) an MPS-MRCISD

computation based on a standard MPS with restricted quantum numbers, and (c) an MPS-MRCISD computation based on an MPS with large sites. Specifically, we compare timings for N_2 with MPS-MRCISD based on a valence CAS(10e,8o), double and triple ζ bases, and different maximal bond dimensions.

The computations are performed with shared-memory parallelism[23] on one node with 28 Intel(R) Xeon(R) E5-2680 v4 CPUs. For each experiment, we start with a random initial state and perform two sweeps with the one-site DMRG algorithm and with perturbative noise.[67,68] For all computations, we measure and compare the total runtimes (including initialization steps such as the setup of the Hamiltonian matrix product operator).

The absolute and relative timings are shown in Figure 3. For the same bond dimension, the MPS-MRCI simulations (full
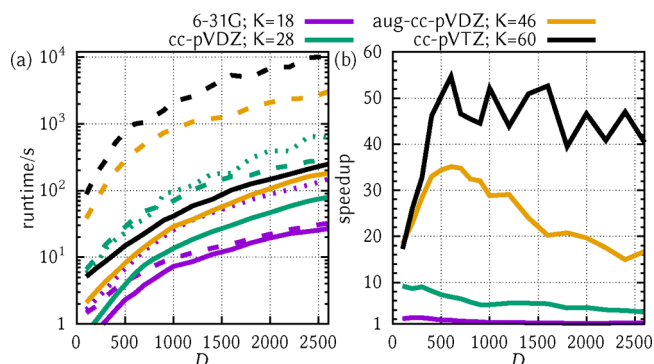

Figure 3. Runtime (left panel) and speedup (right panel) of different MPS-based simulations for N_2 in different bases (total number of orbitals, K are shown). In the left panel, the dashed lines indicate runtimes for an MPS-MRCISD computation with an MPS based on restricted quantum numbers (as many sites as orbitals). The full lines indicate runtimes for the same MRCI setup but with an MPS where the virtual orbitals are collectively described by one large MPS site. The MPS-MRCI computation is based on a valence CAS(10e,8o). The dotted lines indicate runtimes for a normal MPS/DMRG computation, approximating full CI. The right panel shows the speedup of using MPS-MRCI with a large-site MPS over using an MPS with restricted quantum numbers.

and dashed lines) are typically faster than the FCI-based DMRG simulations (dotted lines). This is expected as the Hilbert space size (and thus the matrices in the MPS) are restricted in the MPS-MRCI computation. Likewise, MPS-MRCI simulations converge faster than conventional MPS (FCI) simulations with respect to bond dimension (see below). For all basis sizes the large site MPS (full lines) performs significantly faster than the MPS based on restricted quantum numbers (dashed lines) (right panel in Figure 3). The speedup is always significantly larger than 1, decreases with increasing bond dimension, and increases with basis size. For example, in a triple ζ basis with 60 orbitals, a speedup of more than 50 compared to the standard MPS can be obtained. Notably, the large site MPS computation with a triple ζ basis (60 orbitals; full black line) is faster than the MPS with restricted quantum numbers with a double ζ basis (28 orbitals; dashed green line).

The convergence of the energy versus bond dimension is shown for N_2 in Figure 4. We compute the energy at the equilibrium distance ($R = 1.1208$ Å) using the cc-pVDZ basis. MRCISD is based on a full CAS(14e,10o), employing a
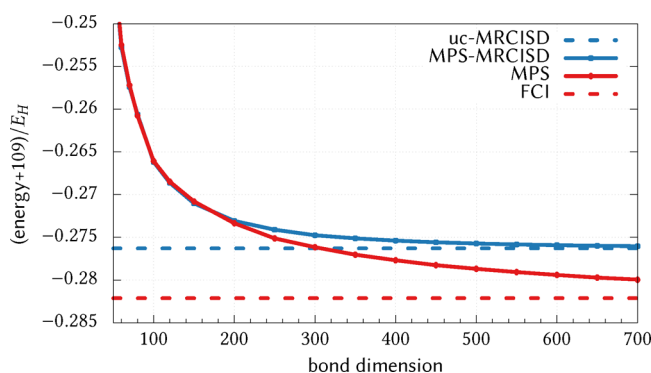
Figure 4. Bond dimension convergence for N_2 at the equilibrium distance. The curves shown are MPS-MRCISD (blue curve) and normal DMRG (red curve). The dashed lines are the converged reference energies.

combination of natural orbitals obtained from CASSCF (for the CAS space) and from Møller−Plesset second-order PT (MP2)[48] (by diagonalizing the one-particle density matrix in the space of the external orbitals). We use the same natural-occupation-based ordering for the MPS-MRCISD and the standard MPS wave functions. While for this example the normal MPS approaches the uc-MRCISD energy more rapidly, namely around $D \sim 300$, the overall convergence with respect to D is slower. Due to the restrictions on the wave function, the MPS-MRCISD method requires a much smaller bond dimension of less than 400 to approach an error of less than 1 mE_H. In contrast, a normal MPS requires a bond dimension of ~ 1000 for a similar convergence tolerance.[70]

4.2. Chromium Dimer. The chromium dimer is a prototypical correlated system with complex bonding, which requires both a multireference treatment and a large amount of dynamic correlation.[51,71−79] Several studies have used both internally contracted and uncontracted MRCISD and related methods to compute the Cr_2 binding curve. Here, we will use the MPS-based formalism to obtain results for several variants of MPS-MRCI methods. Our purpose here is to illustrate the flexibility of the MPS formalism and the utility of the large site implementation which allows us to obtain results in large basis sets and beyond doubles excitations in the MRCI ansatz.

We use a CAS self-consistent field (CASSCF) reference with a valence CAS consisting of 12 electrons and 12 orbitals (3d and 4s shells, 28784 configuration state functions, CSFs) and employ the spin-free exact-2-component Hamiltonian[80,81] with the cc-pV{D,T,Q,5}Z-DK basis sets (up to quintuple ζ), which include up to i-type functions.[82] To decrease the required bond dimension, we use CASSCF natural orbitals and Fiedler ordering in the active space.[83,84] We use standard canonical external and inactive orbitals since an MPS-MRCISD wave function is invariant with respect to orbital rotations in these spaces. We do not employ any BSSE correction. The uncontracted MRCI wave function keeps the 1s, 2s, 2p shells frozen and includes the 3s and 3p orbitals in the inactive space, and we correct the energies using the Pople, and other, size-extensivity corrections. (For comparison, previous uncontracted MRACPF and MRAQCC simulations by Dachsel et al.[85] and Müller[73] used a generalized valence bond reference function consisting of 3088 or 1516 CSFs, using bases with up to h-type functions). The large site representing the external space in the MPS has up to 153×10^3 configurations. The PECs are generated from the binding energies as obtained by

subtracting the energy from the dimer at large distance (to account for size consistency errors). Energy data is given in the Supporting Information.

The MPS-MRCI+Q_P PECs are presented in Figure 5, together with the earlier uc-MRAQCC results from Müller,[73]
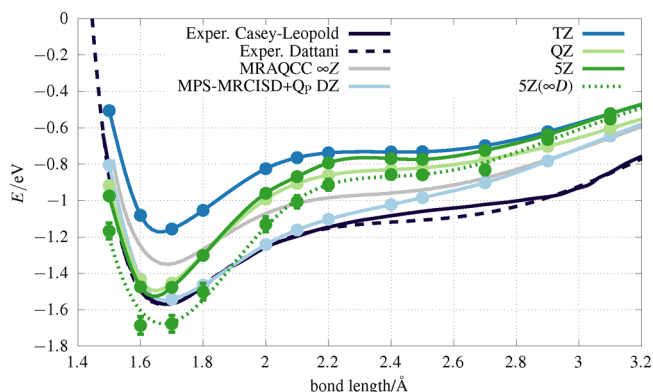

Figure 5. Potential energy curves of the chromium dimer. The black curves show experimental results from Casey and Leopold[86] (full lines) and a different fit to the same data by Dattani et al.[87] (dashed lines). The colored curves show (uncontracted) MPS-MRCISD+Q_P results for different basis sizes (see text for details). The 5ζ result is not fully converged with respect to bond dimension. An approximate extrapolation with bond dimension is shown as the green dotted curve. For reference, the gray curve shows uncontracted MRAQCC(12,12) results in the basis set limit.[73] The MRAQCC PEC correlates fewer electrons and is based on a more restricted reference space.

and experimental curves (with a zero-point energy correction of 0.03 eV[79]). The size consistency error at the 5ζ level is 0.185 eV, which is similar to the uc-MRCI+Q results obtained by Müller.[73] As usual, we computed the size consistency error by taking the difference between the dimer energy at a large distance and twice the energy of the Cr atom (based on restricted open-shell Hartree−Fock orbitals). We find that the MPS-MRCI simulations require a very large bond dimension, typically in the middle of the MPS, which is larger than that required for the reference wave function. The bond dimension at each site is restricted by a density matrix eigenvalue cutoff of 10^{-10} and by the restrictions of possible states that lie in each symmetry sector. The maximum bond dimension required in the MPS representation of the CAS(12,12) wave function is $\sim 1,500$. In contrast, in the MPS-MRCI wave function, the additional external space leads to a dramatic increase of the required bond dimension and with $D = 15,000$ (without spin adaptation) the Qζ PEC is converged to the eye with accuracy of $\lesssim 1$ mE_H. As mentioned in Section 4.1, the required bond dimension still is much smaller than that needed to represent the FCI wave function. However, we could not similarly converge the simulation with the 5ζ basis using a maximum bond dimension of 16,000. In particular, the relative energies for the bond lengths between 2.1 and 2.5 Å and the absolute energies are not converged at that bond dimension, thus we also show an approximate extrapolation to infinite bond dimension[84] for the 5ζ results.

Compared to the experimental curve, the MPS-MRCI+Q_P PECs gives too narrow of a well and the σ-bonding around 2.2 Å is underestimated. The MPS-MRCI+Q results differ significantly from the earlier uc-MRAQCC PEC,[73] which mostly gives a qualitatively better curve, although the different

size-extensivity corrections, basis sets, reference space, and number of correlated electrons makes it difficult to pinpoint the source of the difference.

To see the effect of the size-extensivity correction on the curve shape, we also show the MPS-MRCISD+Q PECs with various corrections for the cc-pVDZ-DK basis in Figure 6.
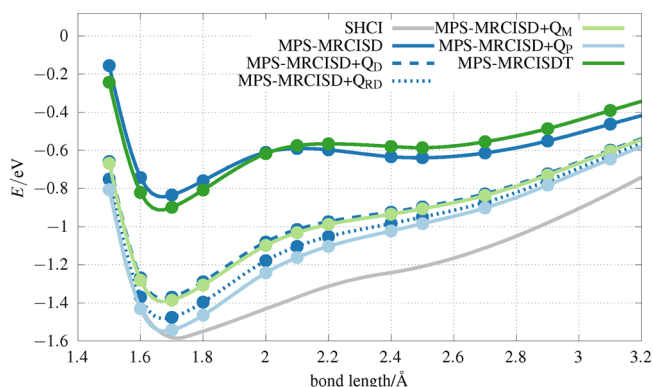

Figure 6. Potential energy curves of the chromium dimer in the cc-pVDZ-DK basis. Shown are MPS-MRCISD, MPS-MRCISD+Q, and MPS-MRCISDT curves. The gray curve shows the selected heat bath configuration interaction (SHCI) result from Li et al.,[79] which approximates the exact PEC in that basis.

Compared to the PEC without any correction (blue curve), the energy is shifted by ~0.8 eV, illustrating the large error of uncorrected MRCISD. All size-extensivity corrections lead to similar curve shapes, differing mostly in the energy shift. For the case of zero inactive orbitals, we found that the MPS-MRAQCC curve resembles the MRCI+Q_P curve. Remarkably, the uncorrected MPS-MRCISD PEC leads to an additional minimum at larger bond distances, which is also the case for other methods such as valence-CAS-based CIPT2, CASPT2, and NEVPT3,[71,73,76] in particular, if small bases are used. For MPS-MRCISD, we found the additional minimum to be more pronounced for larger bases. To estimate the effect of excitations beyond doubles, we additionally converged MPS-MRCISDT results with D = 16,000. The MPS-MRCISDT PEC in the DZ basis only has a very shallow additional minimum and overall displays a qualitatively better PEC, albeit still very different from the more accurate selected heat-bath configuration interaction (SHCI) curve,[79] which approximates FCI. These results indicate that the double minimum observed in MRCI treatments is mainly a size-consistency issue which is corrected by including higher-order excitations explicitly, or a size-consistency correction, which partially accounts for the disconnected higher-order pieces.

4.3. Benzene. In a recent benchmark, the exact energy of the benzene molecule in the cc-pVDZ basis was approximated by a number of methods,[88] arriving at an estimated correlation energy of −863.0 mE_H with an uncertainty of ~1 mE_H. Here, we compare the accuracy of several uncontracted multireference methods implemented using the MPS within the large site formalism. We also provide the variational and extrapolated DMRG energy for comparison. (Results from other methods can be found in refs 88−91, but the DMRG estimate of error, which is an estimate of total error as a fraction of extrapolation error, is most directly comparable to the estimated errors reported here). All simulations use a valence CAS with 30 electrons in 30 orbitals, obtained from an

MPS-CASSCF calculation.[92,93] We use split-localized orbitals with C_s symmetry, obtained from Edmiston-Ruedenberg localization,[94] followed by an additional DMRG-based internal orbital optimization. The large site contains 78 (canonical) orbitals, resulting in ~12×10^3 configurations on the large site for the MPS-MRCISD-type of wave functions (as also used in MRPT2/3) and ~630×10^3 for an MPS-MRCISDT ansatz.

The energies of various methods, based on MPS-MRCISD, MPS-MRCISDT, and MPS-MR perturbation theories and MPS-MRLCCM, are shown in Table 2. We make several

Table 2. Correlation Energies for Benzene, Computed Using Various (Uncontracted) MPS Multireference Methods, Based on a Valence CAS(30, 30)[a]

method	D	ΔE_D/mE_H	ΔE/mE_H	error/mE_H
CCSD(T)			−859.5	
CCSDT			−859.9	
CCSDTQ			−862.4	
DMRG	6000	−859.2	−862.8	0.7
MPS-CASSCF(30,30)	4000	−393.3		
MPS-MRCISD	9000	−808.3	−819.8	2.3
MPS-MRCISD+Q_{RD}	9000	−864.8	−880.7	3.0
MPS-MRCISD+Q_P	9000	−868.0	−884.5	3.3
MPS-MRCISD+Q_M	9000	−857.4	−872.7	3.1
MPS-MRACPF	9000	−869.6	−891.7	4.4
MPS-MRAQCC	9000	−864.0	−875.5	2.3
MPS-MRCISDT	9000	−822.5	−832.5	2.0
MPS-MRREPT2	10000	−857.6	−862.0	0.9
MPS-MRREPT3	10000	−850.1	−854.5	0.9
MPS-MRNEVPT2	10000	−779.3	−783.0	0.7
MPS-MRNEVPT3	10000	−829.9	−834.3	0.9
MPS-MRLCCM	9000	−872.9	−889.9	3.4

[a]Shown are the maximal bond dimension (D), the correlation energy (ΔE_D), the energy extrapolated to infinite bond dimension (ΔE), and its error, defined as 1/5 of its extrapolation distance.[84] Note that the DMRG optimization from ref 88 was performed with spin symmetry included, whereas all MPS-MR-based optimizations were performed without spin symmetry. Thus the MPS-MR methods require a larger bond dimension. The correlation energy is estimated to be around −863 mE_H.[88]

observations. First, the total energies of the MPS-MRCI methods, with size-extensivity corrections, or even with triples, are quite poor. This is likely due to the large number of electrons, which MRCI methods were not designed to treat. Second, the MPS-MRREPT family of perturbation methods yields much better energies than the MPS-MRNEVPT family. MPS-MRREPT2 in particular yields surprisingly accurate energies and is the only MPS-MR method to yield a more accurate estimate than CCSD(T) and CCSDT. Finally, despite the similarity between the MPS-MRLCCM and MPS-MRREPT2 methods, they yield significantly different energies, illustrating the delicate balance needed when choosing the reference Hamiltonian in multireference perturbation theories.

5. CONCLUSIONS

In summary, we have explored the advantages and disadvantages of clustering groups of orbitals into large sites in a matrix product state (MPS) from a computational perspective. While often attractive from a chemical perspective, in many situations clustering leads to an increase in cost because of (1) the underlying exponential scaling of the cluster Hilbert space with

cluster size and (2) longer-range intercluster correlations, which do not allow for a significant decrease in the MPS bond dimension.

A special case however is the MPS with large cluster sites at either end of the MPS. Because each large site only has a single boundary (and does not have a boundary with another large site), when combined with a configuration selection of the large site Hilbert space, there is a large regime of computational advantage. Here we explore the approximation of uncontracted multireference correlation theories using such a large site MPS. We found that the large site MPS formalism yields significant (more than an order of magnitude) computational speedups, compared to a conventional MPS implementation, for multireference wave functions with up to three particles in the external space. General multireference theories are easily realized in this language, as we demonstrate by implementing multireference configuration interaction (MRCI) and MRCI-based size-extensivity-corrected functionals such as averaged quadratic coupled cluster (MRAQCC), various perturbation theories (PTs) such as *n*-electron valence-state PT (NEVPT) and restraining the excitation degree PT (REPT), and the multireference linearized coupled cluster method (MRLCCM).

We use the large site MPS implementation of the above theories to investigate some of the properties of the various multireference treatments in the (a) nitrogen dimer, (b) chromium dimer, and (c) benzene molecule. Our computations used active spaces with up to 30 electrons and 30 orbitals, with up to triple excitations in the external space, and with up to 280 external orbitals. For Cr_2, our results show that the often observed double minimum in the potential energy curve is a result of the neglect of beyond double excitations and can be corrected by their disconnected component (e.g., via size-consistency corrections to MRCI) or the explicit inclusion of triples. For the benzene molecule, we found that among the various theories mentioned, only the multireference REPT2 energy is within 1 mE_H of the estimate of the exact correlation energy. All other theories, including various size-extensivity-corrected MRCISD variants, MRCISDT, MRNEVPT, and MRLCCM, yield poor results showing (1) the need for size-extensive methods and (2) the importance of the choice of the reference Hamiltonian in multireference perturbation theories.

■ APPENDIX

Cluster Matrix Product State for a Hydrogen Chain

Here, we show results for a H_{10} chain, in a cc-pVDZ basis[95] using a cluster MPS with selected configurations within each cluster. The linear nature of H_{10} chains make them very favorable for a description by an MPS, as well as for MPS-based clustering, since the average inter-cluster distance is large. We first discuss a chain of equidistantly spaced H atoms with an atom separation of either 1.1 a_0 (more delocalized) or 1.1 Å (2.08 a_0; more insulating). In the thermodynamic limit, the metal-insulator transition is close to 1.7 a_0, thus the more widely separated system is deep in the insulating regime. The shape of the orbitals is crucial for an efficient cluster MPS. To minimize entanglement, we use a localized basis obtained by aligning H_{10} along the *x* axis and using orbitals that diagonalize $\hat{x}$. These localized orbitals were then grouped into 10 clusters, corresponding to the 10 H atoms. To reduce the required number of configurations, within each cluster, natural orbitals

were obtained by diagonalizing the MP2 one-particle density matrix within the cluster block.

The optimal selection of configurations in a large site can be defined from the exact wavefunction, computing the density matrix of the cluster in the configuration (e.g., determinantal) basis and selecting those corresponding to the largest diagonal elements of the density matrix. Results obtained this way by first approximating the exact wavefunction for the full problem (using the variant of SHCI implemented in PySCF) are denoted "selection based on the full system". We also used a more scalable method where the density matrix of the cluster is approximated using a one-shot two-site density matrix embedding.[96,97] Here, a cluster and a neighboring cluster are chosen as the fragment, and the remaining sites are represented by the density matrix embedding bath. The fragment plus bath problem is then solved via SHCI.[33] Finally, the diagonal of the fragment density matrix is constructed and the configurations corresponding to the largest elements of the density matrix are used for subsequent cluster MPS calculations.

Figure 7 compares the error in the energy as a function of included configurations per site. Compared to selection based
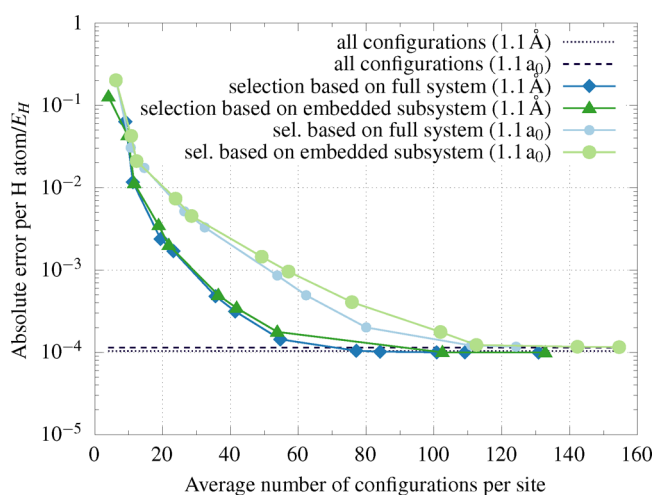
Figure 7. Convergence behavior of configuration selection in a cluster MPS for H_{10}/cc-pVDZ. Shown is the absolute error per H atom versus the average number of configurations per cluster/site. The dark (pale) green and blue curves correspond to a separation of the H atoms of 1.1 Å (1.1 a_0). The configuration selection is either based on the wave function from a selected heat-bath configuration interaction (SHCI) calculation of the full system (blue curves) or based on a SHCI calculation of each subsystem embedded in the full system (green curves); see text for details. The dotted (dashed) line corresponds to the error from a cluster MPS calculation with all 1024 configurations included for a separation of 1.1 Å (1.1 a_0). The remaining error is due to the finite bond dimension.

on the full system, the selection based on the embedded subsystems performs well. To reach an accuracy of $\sim 10^{-3}$ E_H for a separation of 1.1 a_0, $P \sim 50$ configurations per site are required, on average. This corresponds to $\sim 5\%$ of the total number of 1024 possible configurations. In the more stretched geometry with a separation of 1.1 Å, only around 30 configurations are required for a similar accuracy.

To shed light on the possible reduction in bond dimension, we show a convergence plot in Figure 8. Compared to an ordinary MPS, for a given error the bond dimension of the cluster MPS at 1.1 a_0 is reduced by $\sim 12-27\%$. When the interatomic distance is changed from 1.1 a_0 to 1.1 Å, the
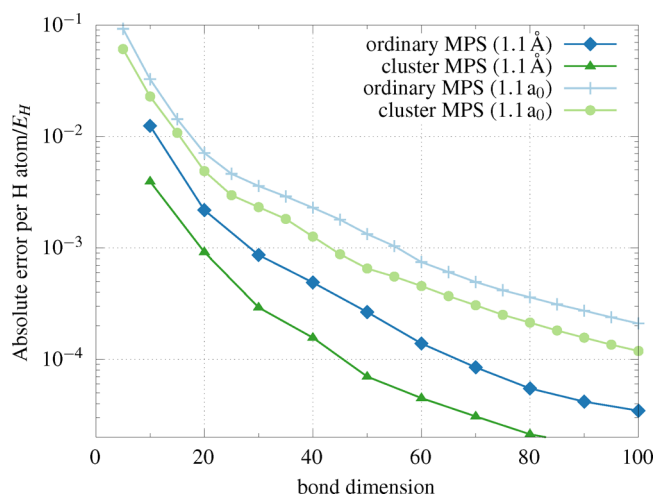
Figure 8. Convergence behavior of the bond dimension in a cluster MPS (blue curves) versus standard MPS (green curves) for H_{10}/cc-pVDZ. The cluster MPS includes all possible configurations. The dark (pale) green and blue curves correspond to a separation of the H atoms of 1.1 Å (1.1 a_0).

reduction in bond dimension increases to ∼30−38%. Note that at the larger distance, far from the insulating transition, the atoms have a clear atomic character. The lack of a large reduction of bond dimension reflects the presence of longer-range correlations, in part from the long-range nature of the Coulomb interaction.

While the small number of configurations per cluster is promising, the reduction in bond dimension is not. Comparing the scaling of an ordinary MPS with a cluster MPS, the computational effort is reduced by introducing clusters if $KD^3 > CD_{cluster}^3 P$. For $P = 50$, this would only be the case if the bond dimension of the cluster MPS, $D_{cluster}$, were reduced by more than 54%. For $P = 30$, the reduction needs to be larger than 45%. Either requirement is not fulfilled at either of the two geometries.

The required bond dimension in a cluster MPS can be better understood by analyzing the singular values σ_i of the site matrix

and the corresponding von Neumann entropy, $-\sum_i \sigma_i^2 \ln(\sigma_i^2)$, at each site in an MPS. The ideal case for a cluster MPS would be to have a very large entropy (large singular values) within each cluster but a small entropy (small singular values) at the boundaries of each cluster. Figure 9 shows this for H_{10} at a separation of 1.1 Å in the cc-pVDZ and cc-pVTZ bases. In contrast to the previous computations, here the localized basis has not been rotated into the natural orbital basis within each cluster. This, however, does not change the analysis of the bond dimension at the cluster boundaries. A decrease at the boundary of each cluster (vertical dashed lines) is only visible for some sites. In agreement with the results from Figure 8, the decrease is only marginal. Increasing the basis, i.e., increasing the amount of long-range (dynamical) correlation that needs to be described, worsens the efficiency of clustering further.

We now discuss a H_{10} chain where 5 molecular H_2 units (with bond distance of 0.74 Å, close to the molecular equilibrium geometry) are separated either by 1.1 or 1.5 Å from each other. Compared to the equidistant separation discussed above, these configurations have H_2 as chemical units, thus there are 5 clusters instead of 10. The larger separation of the H_2 units should favor clustering in the sense of a reduced bond dimension between the clusters, compared to the bond dimension within each cluster. Figure 10 compares the accuracy versus bond dimension for a normal and a cluster MPS. Note that, compared to equidistantly spaced H_{10}, the overall accuracy for a given bond dimension is much higher. At a separation of 1.5 Å, the bond dimension can be reduced by up to ∼44−48%, indicating the more favorable clustering. At the smaller cluster distance of 1.1 Å, the decrease in bond dimension is reduced to ∼36−44%. This is not much different from the equidistant H atom example discussed above. The singular values of the MPSs at each boundary are shown in Figure 11. While the clustering is much more pronounced compared to Figure 9, the decrease of the bond dimension for a particular singular value at the boundary is not dramatic (red contour lines). Note that the first and the last H_2 clusters in H_{10} cannot be resolved in the singular value plot.
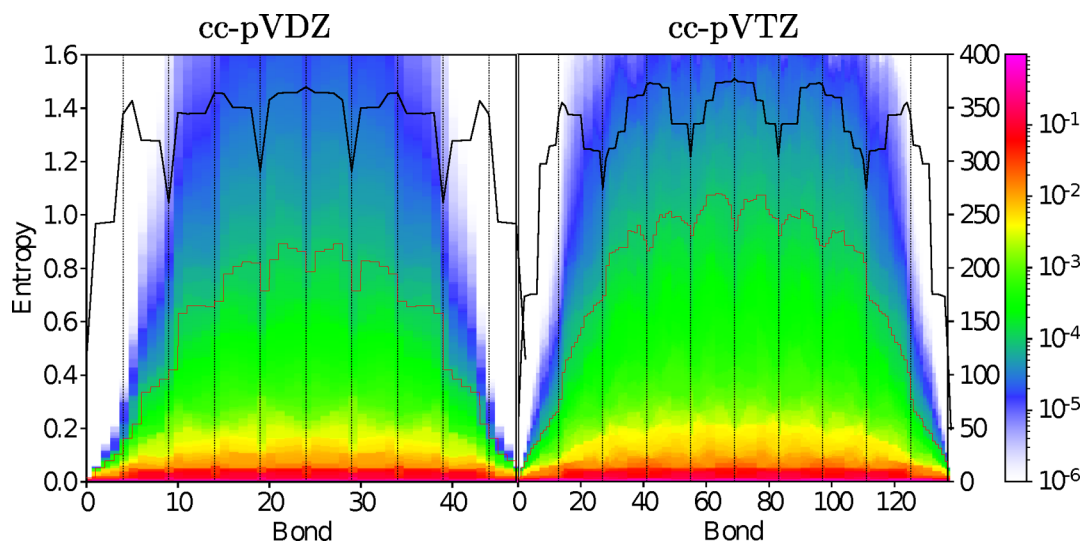

Figure 9. Singular values and von Neumann entropy at different bipartitions in H_{10} (separation 1.1 Å) in a cc-pVDZ basis (left panel) and a cc-pVTZ basis (right panel). The colors corresponds to the magnitude of the singular values σ_i at each bond. The red line denotes the contour at $\sigma = 10^{-4}$. The black line denotes the entropy at the corresponding bipartition. The dashed vertical lines denote the possible cluster decomposition.
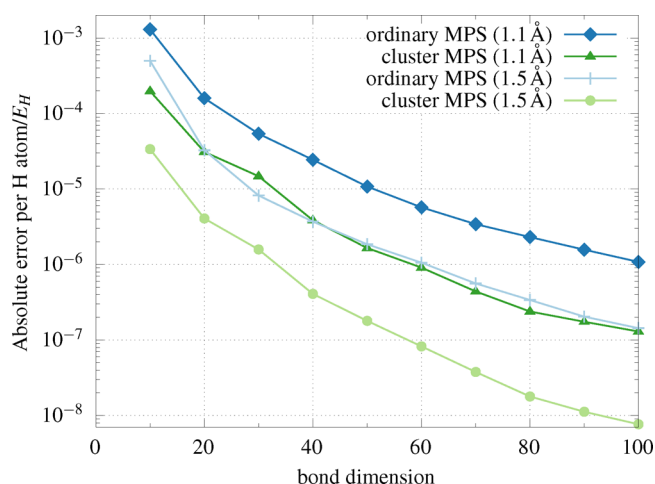
Figure 10. Same as Figure 8 but showing 5 H_2 molecules on a line, separated either 1.1 Å (dark green/blue) or 1.5 Å (pale green/blue) from each other.
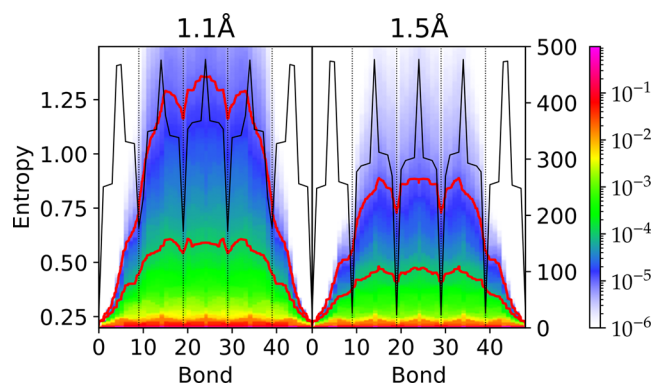

Figure 11. Same as Figure 9 but showing 5 H_2 molecules on a line, separated by either 1.1 Å (left panel) or 1.5 Å (right panel) from each other. The red lines show a contour of the singular values at 10^{-5} (upper lines) and 10^{-4} (lower lines). We here show results for the cc-pVDZ basis.

We note that the simulations performed above are for one-dimensional problems because this is the most favorable setting for the clustering approach. In 1D, the size of the cluster boundary does not scale with the size of the cluster, thus, for sufficiently weak interactions between the clusters, one can expect a regime where the inter-cluster interactions only generate a small number of excitations along the boundary independent of cluster size. The numerical simulations above, however, illustrate that this regime is not always reached in practice, in part due to the long-range of the Coulomb interaction. However, in say two-dimensional lattices (without additional structure) mapped onto one-dimensional slices, then even with local interactions, size-consistency dictates that one needs to retain both an exponential number of configurations per slice and an exponentially growing bond dimension as the system width increases, thus clustering is always asymptotically worse than the standard MPS approach. (See Supporting Information for additional numerical simulations on a 2D hydrogen lattice to illustrate this.) Such general conclusions do not change either under a change of basis (e.g., to a split-localized basis), which simply lead to different constants in the scaling or (in the case of delocalized bases) worse asymptotic behaviour with system size.

■ AUTHOR INFORMATION

Corresponding Authors

Henrik R. Larsson − *Division of Chemistry and Chemical Engineering, California Institute of Technology, Pasadena, California 91125, United States;* ⓞ orcid.org/0000-0002-9417-1518; Email: larsson@caltech.edu

Garnet Kin-Lic Chan − *Division of Chemistry and Chemical Engineering, California Institute of Technology, Pasadena, California 91125, United States;* Email: gkc1000@gmail.com

Authors

Huanchen Zhai − *Division of Chemistry and Chemical Engineering, California Institute of Technology, Pasadena, California 91125, United States*

Klaas Gunst − *Division of Chemistry and Chemical Engineering, California Institute of Technology, Pasadena, California 91125, United States; Center for Molecular Modeling, Ghent University, B-9052 Zwijnaarde, Belgium; Department of Physics and Astronomy, Ghent University, B-9000 Ghent, Belgium;* Present Address: Quantum Simulation Technologies, Inc., Cambridge, MA 02139, United States

Complete contact information is available at:
https://pubs.acs.org/10.1021/acs.jctc.1c00957

Notes

The authors declare the following competing financial interest(s): G.K.C. is a part owner of QSimulate, Inc.

■ REFERENCES

(1) Schollwöck, U. The density-matrix renormalization group in the age of matrix product states. *Ann. Phys.* **2011**, *326*, 96−192.

(2) White, S. R. Density matrix formulation for quantum renormalization groups. *Phys. Rev. Lett.* **1992**, *69*, 2863−2866.

(3) White, S. R. Density-matrix algorithms for quantum renormalization groups. *Phys. Rev. B* **1993**, *48*, 10345−10356.

(4) Chan, G. K.-L.; Sharma, S. The Density Matrix Renormalization Group in Quantum Chemistry. *Annu. Rev. Phys. Chem.* **2011**, *62*, 465−481.

(5) Baiardi, A.; Reiher, M. The density matrix renormalization group in chemistry and molecular physics: Recent developments and new challenges. *J. Chem. Phys.* **2020**, *152*, 040903.

(6) Szalay, S.; Pfeffer, M.; Murg, V.; Barcza, G.; Verstraete, F.; Schneider, R.; Legeza, O. Tensor product methods and entanglement optimization for *ab initio* quantum chemistry. *Int. J. Quantum Chem.* **2015**, *115*, 1342−1391.

(7) Marti, K. H.; Ondík, I. M.; Moritz, G.; Reiher, M. Density Matrix Renormalization Group Calculations on Relative Energies of Transition Metal Complexes and Clusters. *J. Chem. Phys.* **2008**, *128*, 014104.

(8) Kurashige, Y.; Yanai, T. High-Performance *Ab Initio* Density Matrix Renormalization Group Method: Applicability to Large-Scale Multireference Problems for Metal Compounds. *J. Chem. Phys.* **2009**, *130*, 234114.

(9) Kurashige, Y.; Chan, G. K.-L.; Yanai, T. Entangled Quantum Electronic Wavefunctions of the Mn_4CaO_5 Cluster in Photosystem II. *Nat. Chem.* **2013**, *5*, 660−666.

(10) Sharma, S.; Sivalingam, K.; Neese, F.; Chan, G. K.-L. Low-Energy Spectrum of Iron−Sulfur Clusters Directly from Many-Particle Quantum Mechanics. *Nat. Chem.* **2014**, *6*, 927−933.

(11) Li, Z.; Guo, S.; Sun, Q.; Chan, G. K.-L. Electronic Landscape of the P-Cluster of Nitrogenase as Revealed through Many-Electron Quantum Wavefunction Simulations. *Nat. Chem.* **2019**, *11*, 1026−1033.

(12) Li, Z.; Li, J.; Dattani, N. S.; Umrigar, C. J.; Chan, G. K.-L. The Electronic Complexity of the Ground-State of the FeMo Cofactor of Nitrogenase as Relevant to Quantum Simulations. *J. Chem. Phys.* **2019**, *150*, 024302.

(13) Roemelt, M.; Pantazis, D. A. Multireference Approaches to Spin-State Energetics of Transition Metal Complexes Utilizing the Density Matrix Renormalization Group. *Adv. Theory Simul.* **2019**, *2*, 1800201.

(14) White, S. R.; Martin, R. L. *Ab initio* quantum chemistry using the density matrix renormalization group. *J. Chem. Phys.* **1999**, *110*, 4127−4130.

(15) Parker, S. M.; Shiozaki, T. Communication: Active Space Decomposition with Multiple Sites: Density Matrix Renormalization Group Algorithm. *J. Chem. Phys.* **2014**, *141*, 211102.

(16) Li, Z. Expressibility of Comb Tensor Network States (CTNS) for the P-Cluster and the FeMo-Cofactor of Nitrogenase. *Electron. Struct.* **2021**, *3*, 014001.

(17) Nakatani, N.; Chan, G. K.-L. Efficient Tree Tensor Network States (TTNS) for Quantum Chemistry: Generalizations of the Density Matrix Renormalization Group Algorithm. *J. Chem. Phys.* **2013**, *138*, 134113.

(18) Larsson, H. R.; Jiménez-Hoyos, C. A.; Chan, G. K.-L. Minimal Matrix Product States and Generalizations of Mean-Field and Geminal Wave Functions. *J. Chem. Theory Comput.* **2020**, *16*, 5057−5066.

(19) Abraham, V.; Mayhall, N. J. Selected Configuration Interaction in a Basis of Cluster State Tensor Products. *J. Chem. Theory Comput.* **2020**, *16*, 6098−6113.

(20) Nishio, S.; Kurashige, Y. Rank-One Basis Made from Matrix-Product States for a Low-Rank Approximation of Molecular Aggregates. *J. Chem. Phys.* **2019**, *151*, 084110.

(21) Dasgupta, C.; Pfeuty, P. Real-space renormalisation-group study of the one-dimensional Hubbard model. *Journal of Physics C: Solid State Physics* **1981**, *14*, 717.

(22) White, S. R.; Noack, R. M. Real-space quantum renormalization groups. *Physical review letters* **1992**, *68*, 3487.

(23) Zhai, H.; Chan, G. K.-L. Low Communication High Performance Ab Initio Density Matrix Renormalization Group Algorithms. *J. Chem. Phys.* **2021**, *154*, 224116.

(24) Barcza, G.; Werner, M. A.; Zaránd, G.; Legeza, Ö.; Szilvási, T. Towards Large-Scale Restricted Active Space Calculations Inspired by the Schmidt Decomposition. *ArXiv:211106665*, **2021**.

(25) Chan, G. K.-L.; Head-Gordon, M. Highly correlated calculations with a polynomial cost algorithm: A study of the density matrix renormalization group. *J. Chem. Phys.* **2002**, *116*, 4462−4476.

(26) Kolda, T. G.; Bader, B. W. Tensor Decompositions and Applications. *SIAM Rev.* **2009**, *51*, 455−500.

(27) Chepiga, N.; White, S. R. Comb Tensor Networks. *Phys. Rev. B* **2019**, *99*, 235426.

(28) Jimenez-Hoyos, C. A.; Scuseria, G. E. Cluster-Based Mean-Field and Perturbative Description of Strongly Correlated Fermion Systems: Application to the One- and Two-Dimensional Hubbard Model. *Phys. Rev. B* **2015**, *92*, 085101.

(29) Hermes, M. R.; Gagliardi, L. Multiconfigurational Self-Consistent Field Theory with Density Matrix Embedding: The Localized Active Space Self-Consistent Field Method. *J. Chem. Theory Comput.* **2019**, *15*, 972.

(30) Huron, B.; Malrieu, J. P.; Rancurel, P. Iterative Perturbation Calculations of Ground and Excited State Energies from Multi-configurational Zeroth-order Wavefunctions. *J. Chem. Phys.* **1973**, *58*, 5745−5759.

(31) Tubman, N. M.; Lee, J.; Takeshita, T. Y.; Head-Gordon, M.; Whaley, K. B. A Deterministic Alternative to the Full Configuration Interaction Quantum Monte Carlo Method. *J. Chem. Phys.* **2016**, *145*, 044112.

(32) Schriber, J. B.; Evangelista, F. A. Communication: An Adaptive Configuration Interaction Approach for Strongly Correlated Electrons with Tunable Accuracy. *J. Chem. Phys.* **2016**, *144*, 161106.

(33) Holmes, A. A.; Tubman, N. M.; Umrigar, C. J. Heat-Bath Configuration Interaction: An Efficient Selected Configuration Interaction Algorithm Inspired by Heat-Bath Sampling. *J. Chem. Theory Comput.* **2016**, *12*, 3674−3680.

(34) Szalay, P. G.; Müller, T.; Gidofalvi, G.; Lischka, H.; Shepard, R. Multiconfiguration Self-Consistent Field and Multireference Configuration Interaction Methods and Applications. *Chem. Rev.* **2012**, *112*, 108−181.

(35) Langhoff, S. R.; Davidson, E. R. Configuration Interaction Calculations on the Nitrogen Molecule. *Int. J. Quantum Chem.* **1974**, *8*, 61−72.

(36) Pople, J. A.; Seeger, R.; Krishnan, R. Variational Configuration Interaction Methods and Comparison with Perturbation Theory. *Int. J. Quantum Chem.* **1977**, *12*, 149−163.

(37) Meissner, L. Size-consistency corrections for configuration interaction calculations. *Chem. Phys. Lett.* **1988**, *146*, 204−210.

(38) Butscher, W.; Shih, S.-K.; Buenker, R. J.; Peyerimhoff, S. D. Configuration Interaction Calculations for the N_2 Molecule and Its Three Lowest Dissociation Limits. *Chem. Phys. Lett.* **1977**, *52*, 457−462.

(39) Blomberg, M. R. A.; Siegbahn, P. E. M. Singlet and Triplet Energy Surfaces of NiH_2. *J. Chem. Phys.* **1983**, *78*, 5682−5692.

(40) Khait, Y. G.; Jiang, W.; Hoffmann, M. R. On the Inclusion of Triple and Quadruple Electron Excitations into MRCISD for Multiple States. *Chem. Phys. Lett.* **2010**, *493*, 1−10.

(41) Szalay, P. G.; Bartlett, R. J. Multi-reference averaged quadratic coupled-cluster method: a size-extensive modification of multi-reference CI. *Chem. Phys. Lett.* **1993**, *214*, 481−488.

(42) Gdanitz, R. J.; Ahlrichs, R. The averaged coupled-pair functional (ACPF): A size-extensive modification of MR CI(SD). *Chem. Phys. Lett.* **1988**, *143*, 413−420.

(43) Sharma, S.; Chan, G. K.-L. Communication: A flexible multi-reference perturbation theory by minimizing the Hylleraas functional with matrix product states. *J. Chem. Phys.* **2014**, *141*, 111101.

(44) Sharma, S.; Alavi, A. Multireference linearized coupled cluster theory for strongly correlated systems using matrix product states. *J. Chem. Phys.* **2015**, *143*, 102815.

(45) Sharma, S.; Jeanmairet, G.; Alavi, A. Quasi-Degenerate Perturbation Theory Using Matrix Product States. *J. Chem. Phys.* **2016**, *144*, 034103.

(46) Sharma, S.; Knizia, G.; Guo, S.; Alavi, A. Combining Internally Contracted States and Matrix Product States To Perform Multi-reference Perturbation Theory. *J. Chem. Theory Comput.* **2017**, *13*, 488−498.

(47) Guo, S.; Li, Z.; Chan, G. K.-L. A Perturbative Density Matrix Renormalization Group Algorithm for Large Active Spaces. *J. Chem. Theory Comput.* **2018**, *14*, 4063−4071.

(48) Helgaker, T.; Olsen, J.; Jorgensen, P. *Molecular Electronic-Structure Theory*, 1st ed.; Wiley, 2013.

(49) Dyall, K. G. The Choice of a Zeroth-order Hamiltonian for Second-order Perturbation Theory with a Complete Active Space Self-consistent-field Reference Function. *J. Chem. Phys.* **1995**, *102*, 4909−4918.

(50) Angeli, C.; Cimiraglia, R.; Evangelisti, S.; Leininger, T.; Malrieu, J.-P. Introduction of N-Electron Valence States for Multireference Perturbation Theory. *J. Chem. Phys.* **2001**, *114*, 10252−10264.

(51) Angeli, C.; Cimiraglia, R.; Malrieu, J.-P. N-Electron Valence State Perturbation Theory: A Fast Implementation of the Strongly Contracted Variant. *Chem. Phys. Lett.* **2001**, *350*, 297−305.

(52) Angeli, C.; Pastore, M.; Cimiraglia, R. New Perspectives in Multireference Perturbation Theory: The n-Electron Valence State Approach. *Theor. Chem. Acc.* **2007**, *117*, 743−754.

(53) Fink, R. F. Two New Unitary-Invariant and Size-Consistent Perturbation Theoretical Approaches to the Electron Correlation Energy. *Chem. Phys. Lett.* **2006**, *428*, 461−466.

(54) Fink, R. F. The multi-reference retaining the excitation degree perturbation theory: A size-consistent, unitary invariant, and rapidly convergent wavefunction based ab initio approach. *Chem. Phys.* **2009**, *356*, 39−46.

(55) Laidig, W. D.; Bartlett, R. J. A multi-reference coupled-cluster method for molecular applications. *Chem. Phys. Lett.* **1984**, *104*, 424−430.

(56) Laidig, W. D.; Saxe, P.; Bartlett, R. J. The Description of N_2 and F_2 Potential Energy Surfaces Using Multireference Coupled Cluster Theory. *J. Chem. Phys.* **1987**, *86*, 887−907.

(57) Chan, G. K.-L. An algorithm for large scale density matrix renormalization group calculations. *J. Chem. Phys.* **2004**, *120*, 3172−3178.

(58) Kurashige, Y. Multireference Electron Correlation Methods with Density Matrix Renormalisation Group Reference Functions. *Mol. Phys.* **2014**, *112*, 1485−1494.

(59) Olivares-Amaya, R.; Hu, W.; Nakatani, N.; Sharma, S.; Yang, J.; Chan, G. K.-L. The *Ab-Initio* Density Matrix Renormalization Group in Practice. *J. Chem. Phys.* **2015**, *142*, 034102.

(60) Wouters, S.; Van Neck, D. The Density Matrix Renormalization Group for Ab Initio Quantum Chemistry. *Eur. Phys. J. D* **2014**, *68*, 1−20.

(61) Sun, Q.; Berkelbach, T. C.; Blunt, N. S.; Booth, G. H.; Guo, S.; Li, Z.; Liu, J.; McClain, J. D.; Sayfutyarova, E. R.; Sharma, S.; Wouters, S.; Chan, G. K. PySCF: the Python-based simulations of chemistry framework. *WIREs Comput. Mol. Sci.* **2018**, *8*, e1340.

(62) Sun, Q.; Zhang, X.; Banerjee, S.; Bao, P.; Barbry, M.; Blunt, N. S.; Bogdanov, N. A.; Booth, G. H.; Chen, J.; Cui, Z.-H.; Eriksen, J. J.; Gao, Y.; Guo, S.; Hermann, J.; Hermes, M. R.; Koh, K.; Koval, P.; Lehtola, S.; Li, Z.; Liu, J.; Mardirossian, N.; McClain, J. D.; Motta, M.; Mussard, B.; Pham, H. Q.; Pulkin, A.; Purwanto, W.; Robinson, P. J.; Ronca, E.; Sayfutyarova, E. R.; Scheurer, M.; Schurkus, H. F.; Smith, J. E. T.; Sun, C.; Sun, S.-N.; Upadhyay, S.; Wagner, L. K.; Wang, X.; White, A.; Whitfield, J. D.; Williamson, M. J.; Wouters, S.; Yang, J.; Yu, J. M.; Zhu, T.; Berkelbach, T. C.; Sharma, S.; Sokolov, A. Y.; Chan, G. K.-L. Recent developments in the PySCF program package. *J. Chem. Phys.* **2020**, *153*, 024109.

(63) Gunst, K.; Van Neck, D.; Limacher, P. A.; De Baerdemacker, S. The Seniority Quantum Number in Tensor Network States. *SciPost Chem.* **2021**, *1*, 001.

(64) Ma, Y.; Wen, J.; Ma, H. Density-Matrix Renormalization Group Algorithm with Multi-Level Active Space. *J. Chem. Phys.* **2015**, *143*, 034105.

(65) Chan, G. K.-L.; Keselman, A.; Nakatani, N.; Li, Z.; White, S. R. Matrix product operators, matrix product states, and *ab initio* density matrix renormalization group algorithms. *J. Chem. Phys.* **2016**, *145*, 014102.

(66) Kurashige, Y.; Yanai, T. High-performance *ab initio* density matrix renormalization group method: Applicability to large-scale multireference problems for metal compounds. *J. Chem. Phys.* **2009**, *130*, 234114.

(67) White, S. R. Density Matrix Renormalization Group Algorithms with a Single Center Site. *Phys. Rev. B* **2005**, *72*, 180403.

(68) Hubig, C.; McCulloch, I. P.; Schollwöck, U.; Wolf, F. A. Strictly Single-Site DMRG Algorithm with Subspace Expansion. *Phys. Rev. B* **2015**, *91*, 155115.

(69) Larsson, H. R. Computing vibrational eigenstates with tree tensor network states (TTNS). *J. Chem. Phys.* **2019**, *151*, 204102.

(70) Chan, G. K.-L.; Kállay, M.; Gauss, J. State-of-the-Art Density Matrix Renormalization Group and Coupled Cluster Theory Studies of the Nitrogen Binding Curve. *J. Chem. Phys.* **2004**, *121*, 6110−6116.

(71) Celani, P.; Stoll, H.; Werner, H.-J.; Knowles, P. J. The CIPT2 method: Coupling of multi-reference configuration interaction and multi-reference perturbation theory. Application to the chromium dimer. *Mol. Phys.* **2004**, *102*, 2369−2379.

(72) Angeli, C.; Bories, B.; Cavallini, A.; Cimiraglia, R. Third-Order Multireference Perturbation Theory: The n-Electron Valence State Perturbation-Theory Approach. *J. Chem. Phys.* **2006**, *124*, 054108.

(73) Müller, T. Large-Scale Parallel Uncontracted Multireference-Averaged Quadratic Coupled Cluster: The Ground State of the Chromium Dimer Revisited. *J. Phys. Chem. A* **2009**, *113*, 12729−12740.

(74) Kurashige, Y.; Yanai, T. Second-order perturbation theory with a density matrix renormalization group self-consistent field reference function: Theory and application to the study of chromium dimer. *J. Chem. Phys.* **2011**, *135*, 094104.

(75) Guo, S.; Watson, M. A.; Hu, W.; Sun, Q.; Chan, G. K.-L. *N*-Electron Valence State Perturbation Theory Based on a Density Matrix Renormalization Group Reference Function, with Applications to the Chromium Dimer and a Trimer Model of Poly(p-Phenyl-enevinylene). *J. Chem. Theory Comput.* **2016**, *12*, 1583−1591.

(76) Vancoillie, S.; Malmqvist, P. A.; Veryazov, V. Potential Energy Surface of the Chromium Dimer Re-re-revisited with Multiconfigurational Perturbation Theory. *J. Chem. Theory Comput.* **2016**, *12*, 1647−1655.

(77) Luo, Z.; Ma, Y.; Wang, X.; Ma, H. Externally-Contracted Multireference Configuration Interaction Method Using a DMRG Reference Wave Function. *J. Chem. Theory Comput.* **2018**, *14*, 4747−4755.

(78) Purwanto, W.; Zhang, S.; Krakauer, H. An Auxiliary-Field Quantum Monte Carlo Study of the Chromium Dimer. *J. Chem. Phys.* **2015**, *142*, 064302.

(79) Li, J.; Yao, Y.; Holmes, A. A.; Otten, M.; Sun, Q.; Sharma, S.; Umrigar, C. J. Accurate many-body electronic structure near the basis set limit: Application to the chromium dimer. *Phys. Rev. Res.* **2020**, *2*, 012015.

(80) Peng, D.; Reiher, M. Exact Decoupling of the Relativistic Fock Operator. *Theor. Chem. Acc.* **2012**, *131*, 1081.

(81) Kutzelnigg, W.; Liu, W. Quasirelativistic Theory Equivalent to Fully Relativistic Theory. *J. Chem. Phys.* **2005**, *123*, 241102.

(82) Balabanov, N. B.; Peterson, K. A. Systematically Convergent Basis Sets for Transition Metals. I. All-Electron Correlation Consistent Basis Sets for the 3d Elements Sc−Zn. *J. Chem. Phys.* **2005**, *123*, 064107.

(83) Barcza, G.; Legeza, O.; Marti, K. H.; Reiher, M. Quantum-information analysis of electronic states of different molecular structures. *Phys. Rev. A* **2011**, *83*, 012508.

(84) Olivares-Amaya, R.; Hu, W.; Nakatani, N.; Sharma, S.; Yang, J.; Chan, G. K.-L. The *Ab-Initio* Density Matrix Renormalization Group in Practice. *J. Chem. Phys.* **2015**, *142*, 034102.

(85) Dachsel, H.; Harrison, R. J.; Dixon, D. A. Multireference Configuration Interaction Calculations on Cr_2: Passing the One Billion Limit in MRCI/MRACPF Calculations. *J. Phys. Chem. A* **1999**, *103*, 152−155.

(86) Casey, S. M.; Leopold, D. G. Negative Ion Photoelectron Spectroscopy of Chromium Dimer. *J. Phys. Chem.* **1993**, *97*, 816−830.

(87) Dattani, N.; Manni, G. L.; Tomza, M. An improved empirical potential for the highly multi-reference sextuply bonded transition metal benchmark molecule Cr_2. International Symposium on Molecular Spectroscopy, 2017; http://hdl.handle.net/2142/91417.

(88) Eriksen, J. J.; Anderson, T. A.; Deustua, J. E.; Ghanem, K.; Hait, D.; Hoffmann, M. R.; Lee, S.; Levine, D. S.; Magoulas, I.; Shen, J.; Tubman, N. M.; Whaley, K. B.; Xu, E.; Yao, Y.; Zhang, N.; Alavi, A.; Chan, G. K.-L.; Head-Gordon, M.; Liu, W.; Piecuch, P.; Sharma, S.; Ten-no, S. L.; Umrigar, C. J.; Gauss, J. The Ground State Electronic Energy of Benzene. *J. Phys. Chem. Lett.* **2020**, *11*, 8922−8929.

(89) Loos, P.-F.; Damour, Y.; Scemama, A. The Performance of CIPSI on the Ground State Electronic Energy of Benzene. *J. Chem. Phys.* **2020**, *153*, 176101.

(90) Lee, J.; Malone, F. D.; Reichman, D. R. The Performance of Phaseless Auxiliary-Field Quantum Monte Carlo on the Ground State Electronic Energy of Benzene. *J. Chem. Phys.* **2020**, *153*, 126101.

(91) Mahajan, A.; Sharma, S. Taming the Sign Problem in Auxiliary-Field Quantum Monte Carlo Using Accurate Wave Functions. *J. Chem. Theory Comput.* **2021**, *17*, 4786−4798.

(92) Zgid, D.; Nooijen, M. The Density Matrix Renormalization Group Self-Consistent Field Method: Orbital Optimization with the Density Matrix Renormalization Group Method in the Active Space. *J. Chem. Phys.* **2008**, *128*, 144116.

(93) Ghosh, D.; Hachmann, J.; Yanai, T.; Chan, G. K.-L. Orbital Optimization in the Density Matrix Renormalization Group, with Applications to Polyenes and β-Carotene. *J. Chem. Phys.* **2008**, *128*, 144117.

(94) Edmiston, C.; Ruedenberg, K. Localized Atomic and Molecular Orbitals. *Rev. Mod. Phys.* **1963**, *35*, 457−464.

(95) Dunning, T. H. Gaussian basis sets for use in correlated molecular calculations. I. The atoms boron through neon and hydrogen. *J. Chem. Phys.* **1989**, *90*, 1007−1023.

(96) Knizia, G.; Chan, G. K.-L. Density Matrix Embedding: A Simple Alternative to Dynamical Mean-Field Theory. *Phys. Rev. Lett.* **2012**, *109*, 186404.

(97) Knizia, G.; Chan, G. K.-L. Density Matrix Embedding: A Strong-Coupling Quantum Embedding Theory. *J. Chem. Theory Comput.* **2013**, *9*, 1428−1432.